(Received 3 July 2024, Accepted 6 August 2024, Scheduled 20 August 2024)

DMS, CSRR, and DGS Loaded HMSIW Dual-Band Filter with Closely Set Apart Passbands

Gopalakrishnan Soundarya[1], Jayabalan Sam Suresh[2, *], Chinnaswamy Sivamani[3], Doraiswamy Vedha Vinodha[4], Maheleeswaran Pushpavalli[5], Ganesan Vijayakumari[6], and Athappan Senthilkumar[2]

[1]*Department of ECE, Dr. Mahalingam College of Engineering and Technology, Pollachi, Tamil Nadu, India*
[2]*Department of EEE, Dr. Mahalingam College of Engineering and Technology, Pollachi, Tamil Nadu, India*
[3]*Department of Biomedical Engineering, KIT-Kalaignaikarunanidhi Institute of Technology, Coimbatore, India*
[4]*Department of ECE, JCT College of Engineering and Technology, Coimbatore, India*
[5]*Department of ECE, Bannari Amman Institute of Technology, Sathyamangalam, India*
[6]*Department of ECE, Builders Engineering College, Kangayam, India*

ABSTRACT: A Dual-band Half Mode Substrate Integrated Waveguide (HMSIW) filter at 4.88 and 6.42 GHz are shown. Defective Microstrip Structure converts the HMSIW's high-pass response to bandpass. Circular Complementary Split Ring Resonator splits the wide passband to give the filter dual characteristics. The out-of-band properties are improved by using a DS-OCSRR-shaped Defected Ground Structure (DGS). PCB technology is used to build and test the filter using an RT Duroid 5880 substrate with 1.6 mm thickness. The measured and simulated values match. Good skirt selectivity, insertion loss of 1.5/1.42 dB, fractional bandwidths of 9.42% and 6.7%, and return loss profile of 21 dB in both passbands characterize the dual-band filter. The filter is small, measuring $0.86\lambda_g \times 0.37\lambda_g$ at 4.88 GHz.

1. INTRODUCTION

The filters play a crucial part in satellite communication systems. The quality of these filters has a huge impact on the performance of the entire system. The advancement of the communication systems brings forth more design challenges to the filter researchers. In the recent time, dual/multiband filters are in great demand in satellite communication because non-adjacent channels are communicated to the uniform terrestrial area through a single beam. Substrate Integrated Waveguide (SIW) filters, fusion of both planar and non-planar technology, are attractive because of their light weight, low loss, high performance and compact size [1–4]. SIW circuit footprint is more comparable to that of microstrip circuits operating at frequencies below 10 GHz. The footprint of the filter component can be reduced using the Folded SIW [5, 6], Half Mode SIW approach [7–10], and Quarter Mode SIW [11]. Various techniques are used to develop multiband SIW filters. The most commonly used method utilizes several coupling pathways between the input and output ports by cascading numerous individual band filters [12]. In [13], a centre line feeding technique with a by-pass coupling is used to provide narrowband SIW band-pass filter response. Also, higher order modes are utilized to achieve high quality factors. A fourth order quasi-elliptic filter is developed using slot coupling and microstrip cross coupling in the SIW cavity [14]. Even though this technique seems simple, it results in bulkier filter size.

Another technique to achieve multiband operation is by using multimode resonators. In [15], TE_{102} and TE_{201} are resonated to achieve third order directly coupled dual-band filter and fourth order cross coupled dual-band filter. In [16], two degenerate modes of SIW and another resonance by Complementary Split Ring Resonator (CSRR) is utilized resulting in a wide passband. Regrettably, this technique does not fit for multiband filters with relatively separated passbands. Also, to achieve smaller frequency ratio, the circuit size must be compromised.

A further technique is to split a wide passband into multiple bands by inserting transmission zeros (TZs). In [17], a low pass filter is combined with two open stub resonators which creates TZs. The number of stubs determines the number of TZs. In [18], a wideband X/Ku band SIW filter is developed by etching T slots on the top plane. The slots create TZs into the wide passband, thus generating band-pass filter (BPF). In [19], E-shaped Defected Ground Structures (DGSs) connected face to face provide band notch creating a TZ in the high frequency SIW BPF. However, it is challenging for the above filters to get higher order and better passband responses because of the restrictions in the design procedures. In [20], a dual-band HMSIW filter is reported. The filter consists of dual cavity resonators coupled by means of E-shaped slots. Varactor diode is used for tuning the bands. Even though the filter has low loss and tunability, it lacks in selectivity. In [21], dual bands are generated using slot lines and HMSIW resonators. In [22], conventional CSRRs and stepped impedance CSRRs are utilized to

* Corresponding author: Jayabalan Sam Suresh (samsureshjayabalan@gmail.com).

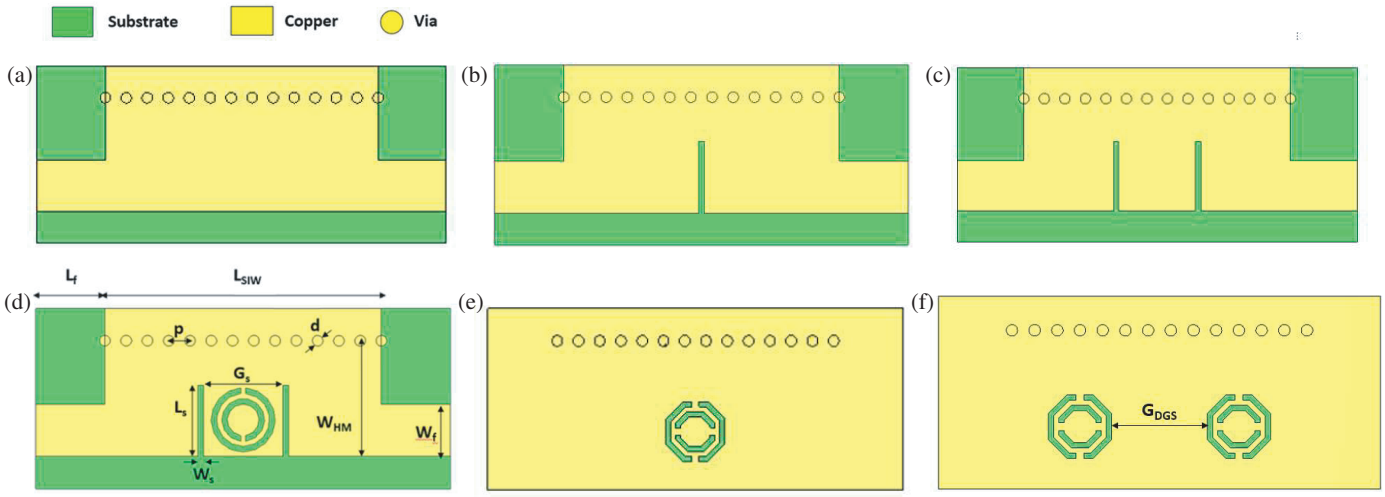

FIGURE 1. (a) HMSIW structure. (b) Single slot engraved on the top plane. (c) Two slots engraved on the top plane. (d) CSRR etched between the slots. (e) Single DS-OCSRR DGS on the bottom plane. (f) Dual DS-OCSRR DGS on the bottom plane (All dimensions in mm, $L_{\text{SIW}} = 26$, $L_f = 6.5$, $W_{\text{HM}} = 11.5$, $p = 2$, $d = 1$, $Ls = 7.45$, $Ws = 0.5$, $Gs = 7.5$, $W_f = 4.9$, $G_{\text{DGS}} = 8.46$).

generate dual-band responses. The filter possesses tunability feature. However, the bands are still not close enough.

A narrow dual-band Half Mode Substrate Integrated Waveguide (HMSIW) BPF with closely spaced passbands and a broad stopband is created in this work. Miniature circuits use HMSIW construction. Slot lines on the top plane of the HMSIW structure operate as a Defective Microstrip Structure (DMS) to provide TZs in its high-pass filtering response. Etching CSRR between DMS slot lines splits the wide passband into two bands. Engraving the Double Split Octagonal CSRR (DS-OCSRR)-inspired DGS on the ground plane improves out-of-band performance. Details are provided on the suggested filter configuration and quality factor computation. The proposed filter's construction and experimental verification are also reported. The proposed filter targets C band satellite communication applications.

2. DESIGN AND ANALYSIS OF THE PROPOSED FILTER CONFIGURATION

2.1. Evolution of the Proposed Filter Configuration

An HMSIW structure is used for the preliminary structure, which has a cutoff frequency of 4.5 GHz. The microstrip lines that are used to feed the structure are matched to 50 Ω. When it comes to the HMSIW structure, the main mode is TE_{10}. To ensure that the electric field is contained within the structure, it is imperative to remember that the pitch of the via holes, denoted as p, must be less than or equal to the diameter of the vias, denoted as d. Figure 1 illustrates the various stages of development that the filter went through. The equations regarding the design are as follows:

$$W_{\text{HM}} = \frac{1}{2} * W_{\text{SIW}} \tag{1}$$

$$W_{\text{SIW}} = a_{\text{eff}} + \frac{d^2}{0.95 * p} \tag{2}$$

$$a_{\text{eff}} = \frac{a}{\sqrt{\varepsilon_r}} \tag{3}$$

$$a = \frac{c}{2f_{c10}} \tag{4}$$

The SIW structure's cutoff frequency in dominant mode is fc_{10}, and waveguide width is a. The effective width of the dielectric filled waveguide is a_{eff}. The width of SIW structure is W_{siw}. The width of the HMSIW structure is W_{HM}.

Figure 2(a) illustrates the S-parameters of the HMSIW structure with a cutoff frequency of 4.5 GHz when it is operated. One of the TZs (TZ_1) in the structure has an attenuation of 28 dB and operates at 3 GHz. Because the symmetrical plane that runs along the transmission line functions as a magnetic wall for the dominant mode, one-half of the SIW structure will continue to have the same electric field pattern as the SIW structure. On display in Figure 2(b) is the E-field distribution at a frequency of 5 GHz.

By etching a slot with a length of $L_s = 0.285\lambda_g$ and a width of $W_s = 0.02\lambda_g$ at the middle of the HMSIW structure, the high-pass character of the HMSIW is transformed into a band-pass response. At the frequency of interest, which is 9 GHz, the guiding wavelength λ_g is computed. This is the frequency at which the transmission zero is projected to occur. Due to the presence of this defective microstrip structure (DMS), the resonance of the HMSIW structure undergoes certain alterations. A representation of the S-parameters of the HMSIW structure with the DMS structure that possesses one TZ at 9 GHz can be found in Figure 3(a). The corresponding electric field distribution is depicted in Figure 3(b), which makes it abundantly evident that the slot excitation causes the signal propagation from one port to the other to be disrupted.

It is necessary to etch a pair of slots on the top plane to enhance the stopband. As a result of the coupling that occurs between the resonators, the frequency peak point of 9 GHz is split into two distinct peaks [23]. For two resonators that are near

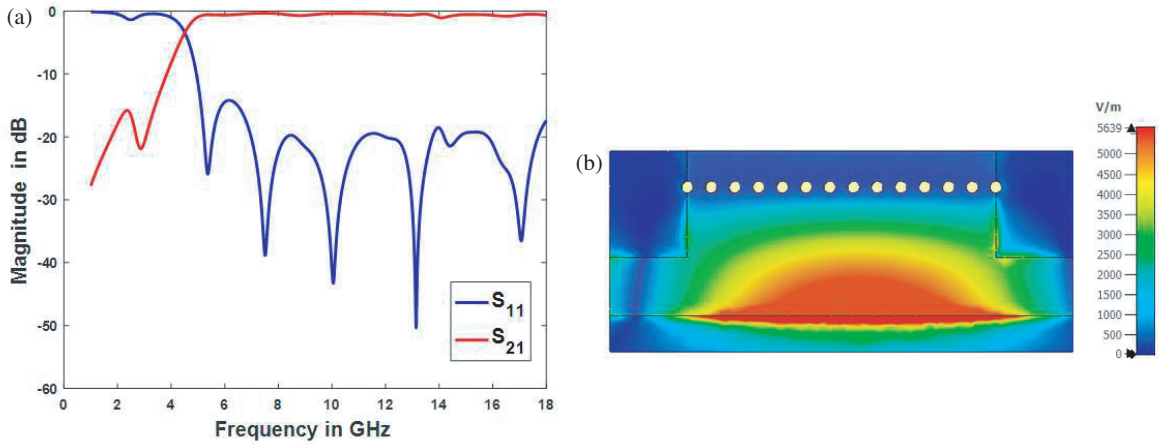

FIGURE 2. (a) S-parameters of the HMSIW structure. (b) E-field distribution at 5 GHz.

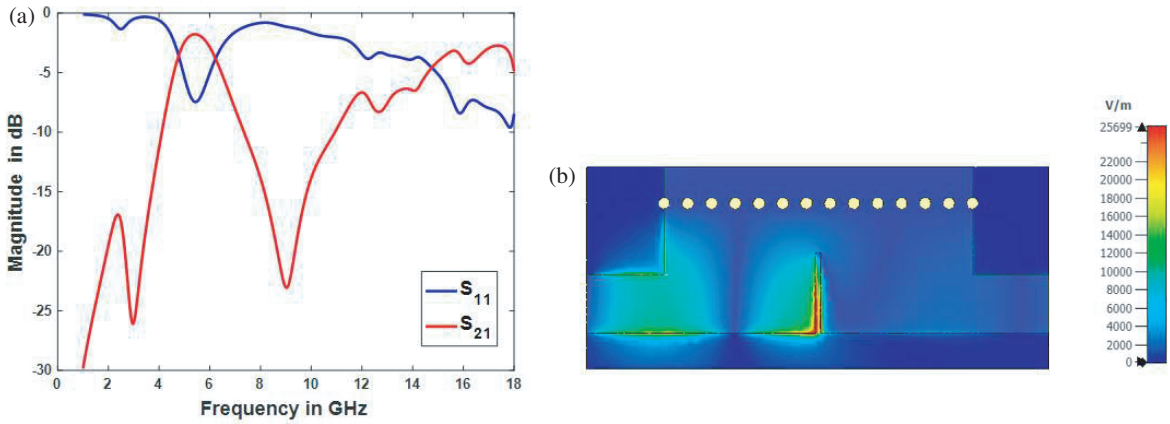

FIGURE 3. (a) S-parameters of the HMSIW structure + single slot. (b) E-field distribution at 9 GHz.

one another, the coupling coefficient can be determined using the EM modelled scattering values of the two resonators as follows:

$$k = \frac{f_2^2 - f_1^2}{f_2^2 + f_1^2} \tag{5}$$

f_1 and f_2 are the lower and upper resonating frequencies of the slot resonator. The scattering parameters of the HMSIW structure with a pair of slots are represented in Figure 4(a).

The TZ frequency of 9 GHz is broken into two different peaks because of the coupling between the slots. Additionally, two TZs occur at 8 GHz and 10 GHz, with an attenuation of 33 dB and 34 dB, respectively. The efficacy of the coupling method is determined by the width of the slot as well as the distance between the two slots. Figure 4(b) illustrates the distribution of the E-field that corresponds to the relevant field.

To achieve dual bands, circular CSRR operating at 6 GHz is designed and incorporated between the two slots in the top plane. CSRR is the negative image of SRR. CSRR exhibits negative permittivity, which when being activated by an axial electric field transforms into an electric dipole. CSRR and SRR possess approximately same resonant frequency. The negative permittivity of the CSRR and its coupling with the slots are responsible for the spacing between the two passbands. The design equations [24] are as follows:

$$f_{\text{CSRR}} = \frac{1}{2\pi\sqrt{L_{eq}C_{eq}}} \tag{6}$$

$$L_{eq} = 0.00508\left[2.303\log\log\left(\frac{4l}{w}\right) - \theta\right] \tag{7}$$

$$C_{eq} = \left[\frac{(\pi r_{avg} - g)\,C_{pul}}{g}\right] + \frac{\varepsilon_0 wt}{2g} \tag{8}$$

$$C_{pul} = \frac{\sqrt{\varepsilon}_e}{cZ_o} \tag{9}$$

$$r_{avg} = R - w - \frac{s}{2} \tag{10}$$

where L_{eq} and C_{eq}, respectively, stand for the overall inductance and capacitance. The total length and width of the wire are represented by 'l' and 'w', respectively. R represents the radius of the outer ring. Spacing between the two rings is specified by 's', and ring thickness is indicated with the notation

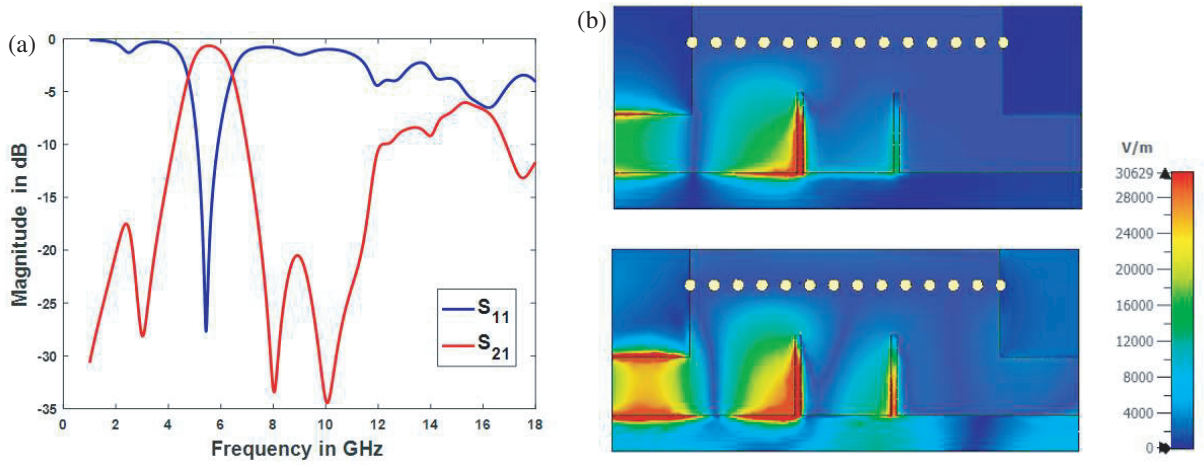

FIGURE 4. (a) S-parameters of the HMSIW structure + Two slots. (b) E-field distribution at 8 GHz (top) and E-field distribution at 10 GHz (bottom).

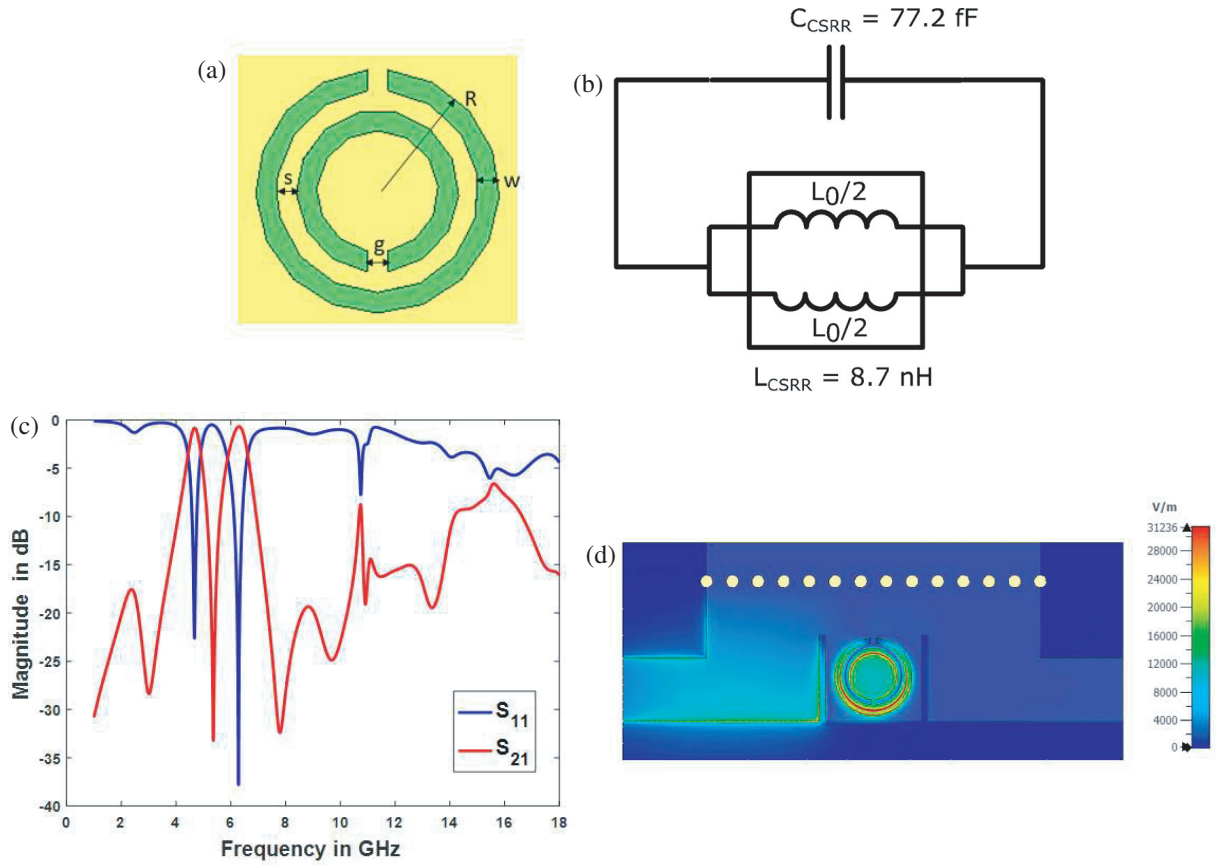

FIGURE 5. (a) CSRR (All dimensions in mm, $R = 3$, $w = 0.5$, $s = 0.5$, $g = 0.5$). (b) Equivalent circuit. (c) S parameters of the HMSIW structure + Two slots + CSRR. (d) E-field distribution at 5.5 GHz.

't'. The split gap is noted by 'g'. C_{pul} is the capacitance in between the loops for unit distance. Z_o is the medium's unit length impedance. θ is the constant with value 2.451 for circular SRR. The velocity of light is denoted by 'c'. Effective permittivity of the medium is noted by ε_e. The geometry of the Circular CSRR is illustrated in Figure 5(a). Its analogous circuit is shown in Figure 5(b).

A stopband is generated within the already existing passband as shown in Figure 5(c). The TZ occurs at 5.5 GHz with 30 dB attenuation. This slight change is due to the coupling between the CSRR and the slot resonators. The electric field pattern at 5.5 GHz is illustrated in Figure 5(d). From the figure, the Circular CSRR responsible for the TZ has maximum field distribution at 5.5 GHz.

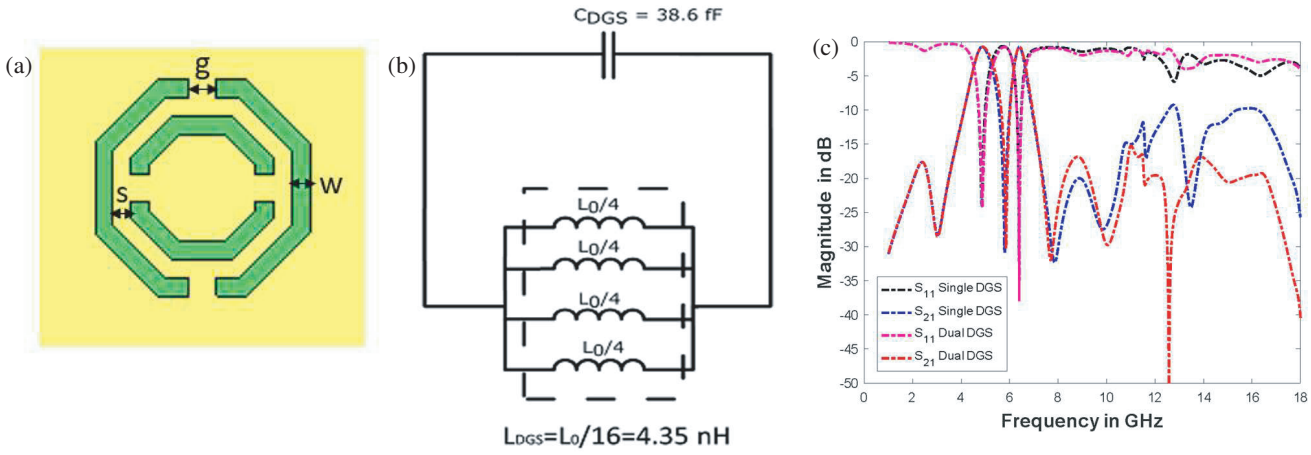

FIGURE 6. (a) DS-OCSRR (All dimesnions in mm, $w = 0.5$, $s = 0.5$, $g = 0.5$). (b) Equivalent circuit. (c) Comparison of the S-parameters of the filter with single DGS and Dual DGS.

In addition, a defect in the shape of a Double Split Octagonal CSRR (DS-OCSRR) is imprinted in the middle of the bottom plane to improve the stopband qualities. It is intended for the DS-OCSRR to function at a frequency of 12 GHz. The resonance frequency of the non bi-anisotropic CSRR is identical to that of the SRR, even though it does not experience cross polarisation effects. With the same geometrical characteristics as the circular CSRR, the double split octagonal CSRR has a resonance frequency that is twice as high as that of its corresponding SRR. Additionally, it can avoid cross polarisation. A representation of the DS-OCSRR and its corresponding circuit may be found in Figure 6(a) and Figure 6(b), respectively. In this context, the letter 'R' stands for the radius of the circular loop that is surrounded by the exterior octagonal ring. Ring width, spacing, and split gap are each represented by the letters 'w', 's', and 'g', respectively.

Alterations are made to the effective capacitance and inductance of the line because of the DGS construction. Considering this, the performance of the stopband has been enhanced; however, there is still opportunity for further development.

The end consequence is that a pair of DGSs that are 8.45 millimeter's apart is utlised. This results in good stopband rejection with an extra TZ at 12.5 GHz and attenuation of 49.7 dB, as shown in Figure 6(c). This is because the transmission line has a greater effective inductance and capacitance than other lines. The mutual coupling that exists between the two DGSs is responsible for the modest alteration that occurs in the shift of the TZ frequency.

2.2. Quality Factor Calculation

The loaded quality factor (Q_l), external quality factor (Q_e), and unloaded quality factor (Q_u) of the filter are defined as follows [25, 26]:

$$Q_l = \frac{f_r}{\Delta f_{3\,\mathrm{dB}}} \tag{11}$$

$$S_{21} = 20 \log \log \left(\frac{Q_l}{Q_e} \right) \tag{12}$$

$$\frac{1}{Q_l} = \frac{1}{Q_u} + \frac{1}{Q_e} \tag{13}$$

Resonant frequency and 3-dB bandwidth are denoted by 'f_r' and '$\Delta f_{3\,\mathrm{dB}}$', respectively. Q_l is found to be 10.61; Q_e is 11.55; and Q_u is 130 for the first passband using formulas (11)–(13). Similarly, for the second passband, Q_l is 14.92; Q_e is 16.27; and Q_u is 180. These quality factors provide insights into the filter's efficiency, selectivity, and resonant behavior, crucial for evaluating its suitability for specific applications and ensuring optimal performance across the desired frequency bands.

3. MEASUREMENT AND RESULTS DISCUSSION

On a Rogers RT/Duroid 5880 board with a thickness of 1.6 millimeters, the HMSIW filter that has been proposed is manufactured. The magnitude of the loss tangent is 0.0009, and the substrate permittivity is 2.2. The software known as Computer Simulated Technology (CST) is utilised for the simulation process, while the Anristu MS 46122B vector network analyzer is utilised for both the experimental verification and the simulation. In Figure 7, you can see an image of the prototype that was manufactured. The overall dimensions of the filter are 0.86 micrograms by 0.37 micrograms, with the λ_g value being determined by calculating the Centre frequency of the first passband.

Figure 8 depicts a comparison of the results of the proposed filter obtained through simulation and those obtained through measurement. There are two passbands that are centered at 4.88 GHz and 6.42 GHz. The bandwidths of these passbands are 0.46 GHz and 0.43 GHz, respectively, which correspond to frequency bandwidths (FBWs) of 9.42% and 6.7%, respectively. At the frequencies of 3.03 GHz, 5.84 GHz, 8 GHz, 10 GHz, and 12.5 GHz, there are five TZs that have been observed, and their respective attenuations are 28 dB, 30 dB, 31 dB, 29 dB, and 49.7 dB. It was discovered that the ratio of bandwidth with a 3 dB bandwidth to a 20 dB bandwidth is 0.23 for the first passband and 0.47 for the second passband. There-

TABLE 1. Comparison with similar reported works.

Ref.	Resonator Structure	CF (GHz)	IL (dB)	FBW (%)	TZs	Size ($\lambda_g \times \lambda_g$)	RL (dB)
[27]	SIW	6.95/7.95	1.47/1.65	2.6/2.3	4	2.2×0.61	17/17
[28]	SIW	3.5/5.24	1.52/1.65	3.14/3.8	2	1.23×1.23	10/10
[29]	HMSIW	5/7.5	1.65/2.25	5.46/4.75	2	1.65×0.93	20/20
		5/8.5	2.02/1.82	6.26/7.75	2	0.84×1.31	20/20
[30]	SIW	5.85/6.15	2.2/2	1.3/1.3	1	2.26×2.26	20/20
[31]	Hybrid	8.05/9.99	1.74/2.21	9.1/6.2	4	1.13×1.02	11.7/11.61
This work	HMSIW+CSRR+DGS	4.88/6.42	1.5/1.42	9.42/6.7	5	0.86×0.37	21/21

Abbreviations: CF — Center Frequency; IL — Insertion Loss; FBW — Fractional Bandwidth; TZs — Transmission Zeros; λ_g — Guided wavelength at the center frequency; RL — Return Loss

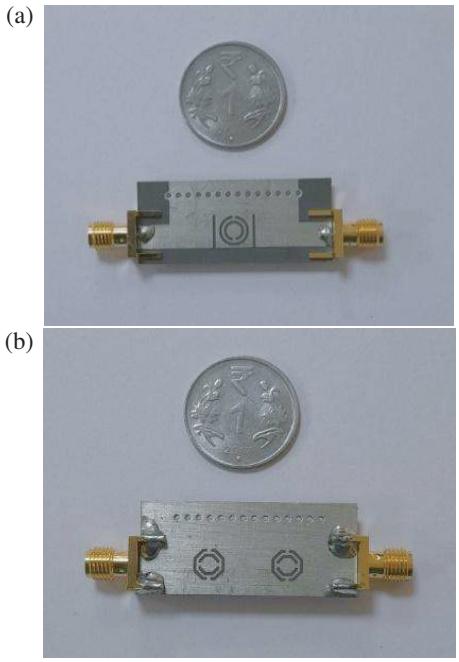

FIGURE 7. Photograph of the (a) top and (b) bottom view of the fabricated prototype.

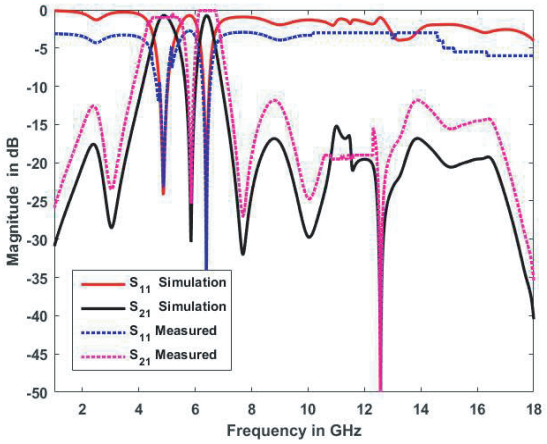

FIGURE 8. Comparison of simulated and measured results of the proposed filter.

fore, the filter has a selectivity that is satisfactory, with an overall rejection that is approximately greater than 30 dB.

In both passbands, the simulated insertion loss is 0.75 dB, whereas the measured values are 1.5 dB and 1.42 dB in the first band and second band, respectively. This bigger loss than the simulated ones can be attributed to the loss of metal, the loss of substrate, and the tolerance of the fabrication process. The return loss that is simulated is 24 decibels in the first passband and 38 decibels in the second passband, respectively. On the other hand, the attenuation value that was measured in both bands is approximately 21 dB. Although there is a slight disparity between the two sets of results, they are highly significant. One of the characteristics of the narrow dual-band filter is its high selectivity and wide stopband response. The filter has a small amount of insertion loss, a decent return loss, a simple design and fabrication process, and it also achieves high stopband performance. Even though the filter has some radiation loss and minimum insertion loss, it has a decent return loss, a simple design and fabrication process, and it also achieves high stopband performance.

The performance characteristics of the proposed filter are compared with those of other current dual-band filters in Table 1. The filter exhibits superior insertion loss, a more favourable return loss profile, and a higher fractional bandwidth than the works cited in [27–31]. The filter has a small size of 0.86 times the wavelength of light in gamma (λ_g) by 0.37 times the wavelength of light in gamma (λ_g).

4. CONCLUSIONS

A miniaturised dual-band HMSIW filter has been designed, built, and tested. The top of the HMSIW construction features engravings of slots and CSRR. The high-pass half-mode substrate integrated waveguide (HMSIW) structure is converted into a band-pass filter (BPF) using slots. The presence of a complementary split ring resonator (CSRR) carved between the slots is responsible for the dual-passband properties. The stopband performance is enhanced by using a Double Split-OCSRR shaped Defected Ground Structure (DGS) on the bottom plane. The filter's equivalent circuit is developed and analysed. The suggested filter, with central frequencird of 4.88 GHz and 6.42 GHz, exhibits minimal insertion loss, a favourable return loss profile, and high selectivity with 5 transmission zeros (TZs). The filter is small, measuring $0.86\lambda_g \times 0.37\lambda_g$, and lightweight, making it very ideal for satellite communication.

REFERENCES

[1] Iqbal, A., J. J. Tiang, S. K. Wong, M. Alibakhshikenari, F. Falcone, and E. Limiti, "Miniaturization trends in substrate integrated waveguide (SIW) filters: A review," *IEEE Access*, Vol. 8, 223 287–223 305, 2020.

[2] Chen, K. F., X. Yang, L. Zhou, and J.-F. Mao, "Miniaturized half-mode T-septum SIW bandpass filter with an ultrawide stopband," *IEEE Microwave and Wireless Components Letters*, Vol. 31, No. 7, 853–856, 2021.

[3] Abdelfattah, M., R. Zhang, and D. Peroulis, "High-selectivity tunable filters with dual-mode SIW resonators in an L-shaped coupling scheme," *IEEE Transactions on Microwave Theory and Techniques*, Vol. 67, No. 12, 5016–5028, 2019.

[4] Iqbal, A., A. W. Ahmad, A. Smida, and N. K. Mallat, "Tunable SIW bandpass filters with improved upper stopband performance," *IEEE Transactions on Circuits and Systems II: Express Briefs*, Vol. 67, No. 7, 1194–1198, 2019.

[5] Muchhal, N. and S. Srivastava, "Design of miniaturized high selectivity folded substrate integrated waveguide band pass filter with Koch fractal," *Electromagnetics*, Vol. 39, No. 8, 571–581, 2019.

[6] Xu, L.-J., J. P. Wang, Y.-X. Guo, and W. Wu, "Double-folded substrate integrated waveguide band-pass filter with transmission zeros in LTCC," *Journal of Electromagnetic Waves and Applications*, Vol. 27, No. 1, 96–103, 2013.

[7] Bozzi, M., A. Georgiadis, and K. Wu, "Review of substrate-integrated waveguide circuits and antennas," *IET Microwaves, Antennas & Propagation*, Vol. 5, No. 8, 909–920, 2011.

[8] Muchhal, N., A. Chakraborty, T. Agrawal, and S. Srivastava, "Miniaturized and selective half-mode substrate integrated waveguide bandpass filter using hilbert fractal for sub-6 GHz 5G applications," *IETE Journal of Research*, Vol. 69, No. 10, 6685–6692, 2023.

[9] He, Z., K. Song, Z. Luo, M. Fan, Y. Zhu, and Y. Fan, "Compact half-mode SIW bandpass filter with high-frequency selectivity," *Electromagnetics*, Vol. 38, No. 2, 96–102, 2018.

[10] You, B., L. Chen, and G. Luo, "The novel reconfigurable double-layer half-mode SIW filter with tunable DMS structure," *Journal of Electromagnetic Waves and Applications*, Vol. 32, No. 14, 1816–1823, 2018.

[11] Iqbal, A., J. J. Tiang, S. K. Wong, S. W. Wong, and N. K. Mallat, "QMSIW-based single and triple band bandpass filters," *IEEE Transactions on Circuits and Systems II: Express Briefs*, Vol. 68, No. 7, 2443–2447, 2021.

[12] Dhwaj, K., X. Li, Z. Shen, and S. Qin, "Cavity resonators do the trick: A packaged substrate integrated waveguide, dual-band filter," *IEEE Microwave Magazine*, Vol. 17, No. 1, 58–64, 2015.

[13] Khan, A. A. and M. K. Mandal, "Narrowband substrate integrated waveguide bandpass filter with high selectivity," *IEEE Microwave and Wireless Components Letters*, Vol. 28, No. 5, 416–418, 2018.

[14] Wong, S.-W., R.-S. Chen, J.-Y. Lin, L. Zhu, and Q.-X. Chu, "Substrate integrated waveguide quasi-elliptic filter using slot-coupled and microstrip-line cross-coupled structures," *IEEE Transactions on Components, Packaging and Manufacturing Technology*, Vol. 6, No. 12, 1881–1888, 2016.

[15] Zhou, K., C.-X. Zhou, and W. Wu, "Substrate-integrated waveguide dual-band filters with closely spaced passbands and flexibly allocated bandwidths," *IEEE Transactions on Components, Packaging and Manufacturing Technology*, Vol. 8, No. 3, 465–472, 2018.

[16] Liu, Z., G. Xiao, and L. Zhu, "Triple-mode bandpass filters on CSRR-loaded substrate integrated waveguide cavities," *IEEE Transactions on Components, Packaging and Manufacturing Technology*, Vol. 6, No. 7, 1099–1105, 2016.

[17] Yang, Q., Y.-C. Jiao, and Z. Zhang, "Compact multiband bandpass filter using low-pass filter combined with open stub-loaded shorted stub," *IEEE Transactions on Microwave Theory and Techniques*, Vol. 66, No. 4, 1926–1938, 2018.

[18] Bhardwaj, P., S. Deivalakshmi, and R. Pandeeswari, "Compact wideband substrate integrated waveguide bandpass filter for X/Ku-band application," *International Journal of RF and Microwave Computer-aided Engineering*, Vol. 31, No. 6, e22634, 2021.

[19] Li, J., Y. Huang, H. Wang, P. Wang, and G. Wen, "38-GHz SIW filter based on the stepped-impedance face-to-face E-shaped DGSS for 5G application," *Microwave and Optical Technology Letters*, Vol. 61, No. 6, 1500–1504, 2019.

[20] Iqbal, A., J. J. Tiang, C. K. Lee, N. K. Mallat, and S. W. Wong, "Dual-band half mode substrate integrated waveguide filter with independently tunable bands," *IEEE Transactions on Circuits and Systems Ii: Express Briefs*, Vol. 67, No. 2, 285–289, 2019.

[21] Chen, F., K. Song, B. Hu, and Y. Fan, "Compact dual-band bandpass filter using HMSIW resonator and slot perturbation," *IEEE Microwave and Wireless Components Letters*, Vol. 24, No. 10, 686–688, 2014.

[22] Huang, Y. M., Y. Peng, Y. Zhou, H. Jin, S. Leng, and G. Wang, "Size-reduced dual-band HMSIW cavity filters loaded with double-sided SICSRRs," *Electronics Letters*, Vol. 53, No. 10, 689–691, 2017.

[23] Wang, Y., W. Hong, Y. Dong, B. Liu, H. J. Tang, J. Chen, X. Yin, and K. Wu, "Half mode substrate integrated waveguide (HMSIW) bandpass filter," *IEEE Microwave and Wireless Components Letters*, Vol. 17, No. 4, 265–267, 2007.

[24] Saha, C. and J. Y. Siddiqui, "A comparative analyis for split ring resonators of different geometrical shapes," in *2011 IEEE Applied Electromagnetics Conference (AEMC)*, 1–4, Kolkata, India, 2011.

[25] Papapolymerou, J., J.-C. Cheng, J. East, and L. P. Katehi, "A micromachined high-Q X-band resonator," *IEEE Microwave and Guided Wave Letters*, Vol. 7, No. 6, 168–170, 1997.

[26] Hill, M. J., R. W. Ziolkowski, and J. Papapolymerou, "A high-Q reconfigurable planar EBG cavity resonator," *IEEE Microwave and Wireless Components Letters*, Vol. 11, No. 6, 255–257, 2001.

[27] Yang, Z., B. You, and G. Luo, "Dual-/tri-band bandpass filter using multimode rectangular SIW cavity," *Microwave and Optical Technology Letters*, Vol. 62, No. 3, 1098–1102, 2020.

[28] Li, P., H. Chu, D. Zhao, and R. S. Chen, "Compact dual-band balanced SIW bandpass filter with improved common-mode suppression," *IEEE Microwave and Wireless Components Letters*, Vol. 27, No. 4, 347–349, 2017.

[29] Zhou, K., C.-X. Zhou, and W. Wu, "Dual-mode characteristics of half-mode SIW rectangular cavity and applications to dual-band filters with widely separated passbands," *IEEE Transactions on Microwave Theory and Techniques*, Vol. 66, No. 11, 4820–4829, 2018.

[30] Rezaee, M. and A. R. Attari, "A novel dual mode dual band SIW filter," in *2014 44th European Microwave Conference*, 853–856, Rome, Italy, 2014.

[31] Zhu, Y. and Y. Dong, "A compact dual-band quasi-elliptic filter based on hybrid SIW and microstrip technologies," *IEEE Transactions on Circuits and Systems Ii: Express Briefs*, Vol. 69, No. 3, 719–723, 2021.